UNNS Substrate Research Program | UNNS-H Mode Project | Working Manuscript

Boundary-Route Preservation in H-Mode Plasma: A UNNS Edge-Admissibility Analysis of TCV and TokaMark Data

Instruments: STRUC-PERC-I v2.5.0 · STRUC-I v1.0.4

Corpus: TCV Zenodo 14996664 ($N = 92$ events) · TokaMark/MAST public arrays (5 physical-window shots)

Data: TCV L-H threshold database; TokaMark HTTP diagnostic arrays

Research corpus: UNNS-H Mode Project computational archive [C1]

Status: TCV event validation complete · full corpus extension complete · TokaMark physical-window recovery gate passed · 2026

Abstract

H-mode plasma confinement can be represented as a boundary-route preservation transition in which the plasma edge moves from a fragmentation-dominated leakage state toward an admissible route-preserving state, and this transition is empirically reflected in UNNS edge-admissibility margins across TCV event corridors and TokaMark physical windows. We define an event-level edge-admissibility margin $m_{\text{edge,event}} = C_{\text{edge}} - F_{\text{route}}$, where F_{route} captures power-balance, transport, and timing fragmentation pressures and C_{edge} captures edge-response, density, geometry, and species capacity terms. A manually reviewed nine-shot TCV subset separates into three strictly non-overlapping structural corridors: negative leakage ($n = 4$, mean -0.458), boundary ambiguous ($n = 2$, mean -0.011), and positive boundary ($n = 3$, mean $+0.660$), with the positive corridor defined by edge-response dominance rather than total heating power. A tag-free generalization across the full 92-event TCV canonical corpus preserves three-corridor structure with a statistically significant ILH association (AUC = 0.690, permutation $p = 0.0022$), though standard plasma variables remain superior for binary ILH prediction. A time-resolved extension to TokaMark/MAST public data constructs a diagnostic-confidence-corrected margin $m_{\text{edge,conf}}(t)$ and applies physical-window hardening (HARDENED_v0.2). The resulting window analysis recovers the expected ordering L_MODE < LH_TRANSITION < H_MODE_STABLE under $m_{\text{edge,conf}}$, with positive within-shot H-minus-L deltas in all five recovered H-mode-stable cases (range +1.062 to +1.326). These results establish a first empirical UNNS formulation of H-mode as boundary-route preservation, ready for broader external anchoring and cross-machine validation.

Contents

1 Introduction

H-mode is the most important confinement regime for magnetic fusion energy. It is characterized by a sudden improvement in energy confinement when heating power crosses a threshold P_{LH}, the formation of a sharp edge temperature pedestal, an edge transport barrier, and an approximately twofold increase in energy confinement time relative to L-mode. The transition from L-mode to H-mode, the L-H transition, is reproducibly observed across tokamaks and stellarators, yet its physical origin remains an active subject of study.

Standard accounts of the L-H transition emphasize radial electric field formation, $E \times B$ velocity shear, turbulence suppression, and the role of the ion heat channel near threshold. These mechanisms are physically well-motivated and experimentally constrained. What they share is a description of the transition in terms of changes in local plasma quantities: temperatures, densities, electric fields, and turbulence levels.

The present work proposes a complementary structural account. Within the UNNS (Unbounded Nested Number Sequences) Substrate framework, confinement is related to the admissibility of boundary routes: structural configurations along which energy and particle fluxes are organized. L-mode is characterized by a leakage-like structure in which route-fragmentation pressure exceeds edge-preserving capacity. H-mode is characterized by a boundary-admissible structure in which edge-response capacity is sufficient to organize and preserve confinement routes.

This paper introduces the **edge-admissibility margin** $m_{\mathrm{edge}} = C_{\mathrm{edge}} - F_{\mathrm{route}}$ as an empirical instrument for measuring this balance, applies it to TCV event-level data and time-resolved TokaMark/MAST diagnostic arrays, and reports the outcome of a physical-window analysis that recovers the expected structural ordering across L-mode, L-H transition, and H-mode-stable windows.

This manuscript is a plasma-domain continuation of the UNNS boundary and admissibility program. Prior UNNS work established admissibility [U1, U2], percolative realizability [U3], connectivity margins and boundary geometry [U5, U6], the margin-confinement law [U7], and boundary-route preservation as a structural tool for analyzing physical systems [U8, U9]. The present work applies that theoretical sequence to magnetically confined plasma by treating the L-H transition as a boundary-admissibility crossing and H-mode as a route-preserving edge state.

The manuscript is organized as follows. Section 2 develops the conceptual framework: Sections 2.1–2.2 introduce route fragmentation, edge capacity, and the L-H transition as an admissibility crossing, while Section 2.3 relates the plasma formulation to the Charge Boundary-Route Preservation Law. Section 3 defines the formal model. Section 4 presents the nine-shot TCV event-level results. Section 5 presents the full 92-event corpus extension. Section 6 introduces the TokaMark time-resolved extension and diagnostic-confidence correction. Section 7 describes physical-window construction and hardening. Section 8 presents the main physical-window result. Section 9 interprets the results. Section 10 states limitations and next steps. Section 11 concludes.

This paper makes four contributions: (i) it formulates H-mode as boundary-route preservation in the UNNS substrate, introducing the structural interpretation of the L-H transition as an admissibility crossing; (ii) it defines an event-level edge-admissibility margin and validates strict corridor ordering in a reviewed nine-shot TCV subset; (iii) it extends the margin to the full 92-event TCV corpus and quantifies the ILH association relative to standard plasma variables; and (iv) it constructs a diagnostic-confidence-corrected time-window margin on public TokaMark/MAST data that recovers the ordering L_MODE < LH_TRANSITION < H_MODE_STABLE with positive within-shot H-minus-L deltas in all five recovered H-mode-stable cases.

The complete computational research corpus for this manuscript is released as the UNNS-H Mode Project archive [C1]. The archive contains the adapters, processed canonical data, STRUC-I and STRUC-PERC-I chamber inputs, analysis components, validation scripts, reports, dashboards, manifests, and output summaries used to generate the results reported here. The manuscript should therefore be read together with the research corpus as a reproducible computational object rather than as a standalone theoretical note.

1.1 Structural Claim versus Predictive Claim

This manuscript makes a *structural* claim, not a *predictive* one. A predictive model asks whether ILH= 1 can be classified or forecast given input measurements. A structural coordinate asks whether observed states are organized into coherent, interpretable regimes that reflect an underlying physical balance.

The two are different tasks with different success criteria. Section 5 reports that standard plasma variables already classify ILH at LOO AUC = 1.000 on the 92-event TCV corpus. The UNNS margin does not improve that classification. That is the correct outcome for a structural coordinate: it is not designed to beat a power-threshold predictor. It is designed to reveal why some ILH= 1 events sit in the negative leakage corridor (Shots 67992 and 68001: high transport and power-balance pressure despite an H-mode indicator), while others sit in the positive boundary corridor (Shots 66445, 69892, 68719: edge-response dominance with low fragmentation pressure). That distinction is not visible to a binary ILH classifier. The structural claim is that this difference is physically meaningful.

2 Conceptual Framework: Boundary-Route Preservation

2.1 Route Fragmentation and Edge Capacity

Within the UNNS substrate framework [U1, U2, U3], a physical boundary is characterized by the balance between *route-fragmentation pressure* and *edge-preserving capacity*. Route fragmentation arises when the structural load on a boundary — from heating, transport, or temporal instability — exceeds the capacity of the edge region to organize and maintain confinement routes. Edge capacity arises from structural features of the edge that stabilize or preserve routes: edge-response signatures, density support, ion species context, and magnetic geometry.

Definition 2.1 (Route Fragmentation)**.** Route fragmentation is the structural condition in which confinement-route integrity is disrupted by power-balance, transport, or timing pressures that exceed the edge's organizing capacity.

Definition 2.2 (Edge Admissibility)**.** A plasma edge is admissible when its structural configuration lies within the region of the UNNS admissibility manifold $\mathcal{M}_{\mathrm{adm}}$ [U5, U6] compatible with sustained route preservation. The edge is non-admissible when fragmentation pressure dominates.

2.2 The L-H Transition as an Admissibility Crossing

In this framework, the L-mode state is characterized by $F_{\text{route}} > C_{\text{edge}}$: fragmentation pressure exceeds edge capacity, and the plasma edge behaves as a leakage layer. The H-mode state is characterized by $C_{\text{edge}} > F_{\text{route}}$: edge-response structure is sufficiently organized to preserve confinement routes. The L-H transition corresponds to the crossing $F_{\text{route}} \approx C_{\text{edge}}$, a passage through the boundary of the admissibility region.

This does not reject classical plasma quantities. Power, density, transport, and geometry all appear as components of F_{route} and C_{edge}. The structural account reorganizes them into a *balance* [U7, U8, U9]: instead of asking whether power exceeds a threshold, it asks whether edge-organizing capacity is sufficient to sustain route preservation against the combined fragmentation pressure from all channels.

The conceptual map is summarized in Table 1.

Table 1: Translation map between plasma terms and UNNS structural terms.

Plasma term	**UNNS term**	**Model component**
L-mode turbulence	Low-margin leakage regime	$F_{\text{route}} > C_{\text{edge}}$
Power threshold P_{LH}	Route-fragmentation driver	S_{pb}, S_{tr}
L-H transition	Admissibility threshold crossing	$m_{\text{edge}} \approx 0$
Edge transport barrier	Boundary-route preservation layer	S_{er} dominant
H-mode candidate event	Positive boundary margin (event)	$m_{\text{edge,event}} > 0$
E×B shear suppression	Route-reordering mechanism	S_{er} proxy
Radial geometry q_{95}, κ, δ	Route stabilization geometry	geometry stability
Candidate divertor/edge signal	Edge-response signature	S_{er}

2.3 Relation to Charge Boundary-Route Preservation

The present plasma-boundary formulation is the confinement-domain analogue of the Charge Boundary-Route Preservation Law [U9, U16]. In the charge-domain formulation, scalar charge conservation is necessary but not sufficient for structural admissibility. A charge-bearing transition must also preserve a coherent boundary-route transformation between the initial and final charge-bearing structures. Charge balance is the visible projection; boundary-route preservation is the structural invariant.

The H-mode problem has the same structural form. Standard plasma analysis identifies threshold access through heating power, density, geometry, and the binary L-H indicator. These quantities are indispensable, but they do not by themselves determine the structural route by which the plasma edge enters, fails to enter, or temporarily occupies a confinement-preserving state. A shot may carry an H-mode indicator while still lying in a fragmentation-loaded boundary configuration. Conversely, a positive-boundary corridor may indicate an edge-response-dominant route-preserving configuration. Thus, just as equal scalar charge does not imply equal charge route, equal H-mode access does not imply equal edge-route structure.

The analogy is summarized in Table 2.

Table 2: Analogy between charge boundary-route preservation and plasma edge-route preservation.

Charge-boundary formulation	Plasma H-mode formulation
Scalar charge Q	Threshold power, ILH label, or H-mode access indicator
Charge balance $Q_i = Q_f$	Threshold access or observed L-H transition
Route/closure coherence	Edge-route preservation
Route-incoherent charge-balanced transition	Fragmentation-loaded H-mode access
Forbidden or constrained boundary pressure	Leakage-dominated or non-admissible edge pressure
Boundary-route preservation	Route-preserving edge admissibility

In the charge law, the structural lift has the form

$$Q \mapsto (Q, L, R, C, B, \Sigma),$$

where Q is the visible charge projection and the remaining coordinates encode layer, route class, closure class, boundary status, and composition. In the plasma setting, the corresponding lift is

$$\text{H-mode access} \mapsto (F_{\text{route}}, C_{\text{edge}}, m_{\text{edge,event}}, \text{margin state}, \text{diagnostic support}),$$

where F_{route} measures route-fragmentation pressure and C_{edge} measures edge-preserving capacity. The event-level edge-admissibility margin

$$m_{\text{edge,event}} = C_{\text{edge}} - F_{\text{route}}$$

is therefore the plasma analogue of the route/closure admissibility coordinate: it separates the visible event label from the boundary route by which that event is realized.

Principle 2.3 (Plasma Boundary-Route Preservation)**.** H-mode access is a visible projection of a deeper edge-route transformation. Threshold access or binary H-mode classification is necessary evidence, but it is not sufficient to characterize the boundary state. A route-preserving H-mode state requires edge capacity to dominate route-fragmentation pressure, producing a positive edge-admissibility margin.

This principle explains the structural role of the three margin states introduced below. A negative margin identifies a boundary state in which fragmentation pressure dominates capacity. A boundary-ambiguous margin identifies the transition neighborhood where

$$F_{\text{route}} \approx C_{\text{edge}}.$$

A positive margin identifies a route-preserving admissible configuration in which edge capacity dominates route-fragmentation pressure. The L-H transition is therefore not only a threshold crossing; in the UNNS representation, it is a change in the admissibility status of edge routes.

This relation also clarifies the role of Section 1.1. The H-mode analysis is not designed to replace standard plasma variables or to outperform them in binary ILH classification. It lifts the visible event label into a boundary-route coordinate system. In that lifted representation, binary H-mode access alone cannot distinguish fragmentation-loaded access from edge-response-dominant route preservation.

In compact form, the repeated UNNS pattern is:

$$\text{value is projection,} \qquad \text{route is structure,} \qquad \text{boundary preservation is admissibility.}$$

For the charge domain, this appears as charge balance plus route/closure coherence. For the plasma domain, it appears as threshold access plus edge-route preservation. Balance alone is not enough.

3 Formal Model: Event-Level Edge-Admissibility Margin

3.1 Model Definition

Definition 3.1 (Event-Level Edge-Admissibility Margin [U5, U7])**.** The event-level UNNS edge-admissibility margin is

$$m_{\text{edge,event}} \;=\; C_{\text{edge}} - F_{\text{route}}, \tag{1}$$

where F_{route} is the route-fragmentation pressure and C_{edge} is the edge-preserving capacity, both normalized to $[0, 1]$.

3.2 Route Fragmentation

The route-fragmentation pressure is constructed as a weighted mean of three score components:

$$F_{\text{route}} \;=\; 0.35\, S_{\text{pb}} \;+\; 0.35\, S_{\text{tr}} \;+\; 0.30\, S_{\text{ti}}, \tag{2}$$

where:

- S_{pb}: power-balance score — power imbalance relative to the L-H threshold (P_{total}, P_{loss} levels);
- S_{tr}: transport score — effective transport elevation (χ_{eff}, P_{loss} pressure);
- S_{ti}: timing score — transition-event timing spread (multi-time fragmentary structure).

3.3 Edge Capacity

The edge-preserving capacity is constructed as a weighted mean of four terms:

$$C_{\text{edge}} \;=\; 0.45\, S_{\text{er}} \;+\; 0.25\, \rho_{\text{dens}} \;+\; 0.15\, \gamma_{\text{geom}} \;+\; 0.15\, \sigma_{\text{sp}}, \tag{3}$$

where:

- S_{er}: edge-response score — candidate divertor/edge signal (proxy for $E \times B$ suppression signature);
- ρ_{dens}: density support percentile relative to the Ryter threshold;
- γ_{geom}: geometry stability from q_{95}, κ, δ;
- σ_{sp}: species position (H/He ion fraction context).

Box 1. Candidate Edge-Response Signal

S_{er} is a composite candidate edge-response proxy, not a direct E_r or $E \times B$ measurement. It is constructed from the following candidate channels available in the TCV Zenodo corpus and TokaMark/MAST diagnostic arrays:

• `divertor_signal_candidate`	candidate divertor/edge emission signal
• `divertor_signal_150_candidate`	150 ms rolling window variant
• edge-profile sharpening	inferred from T_e gradient proxy
• soft-X emission consistency	used in TokaMark window labeling
• divertor-state or edge-emission change	transition-local context field

The source field `divertor_signal_candidate` is confirmed as the primary quantitative carrier of S_{er} in the TCV corpus. Whether it captures the D-alpha suppression signature, a related divertor recycling signal, or another edge-emission proxy requires source-notebook verification beyond the scope of this manuscript. Direct validation of S_{er} against E_r, $E \times B$ shear, pedestal-gradient evolution, or turbulence diagnostics remains future work.

3.4 Margin States

The margin $m_{\mathrm{edge,event}}$ is mapped to three structural states:

Definition 3.2 (Margin States [U3, U6]).

$$\text{Negative leakage margin:} \quad m_{\mathrm{edge,event}} < -0.10 \tag{4}$$

$$\text{Boundary ambiguous margin:} \quad -0.10 \le m_{\mathrm{edge,event}} \le +0.10 \tag{5}$$

$$\text{Positive boundary margin:} \quad m_{\mathrm{edge,event}} > +0.10 \tag{6}$$

The negative leakage margin corresponds to a structurally leakage-like or stressed event. The positive boundary margin corresponds to edge-response dominance. Neither state is a binary H-mode classifier.

3.5 Time-Resolved Extension

The time-resolved margin is defined analogously:

$$m_{\mathrm{edge}}(t) = C_{\mathrm{edge}}(t) - F_{\mathrm{route}}(t), \tag{7}$$

computed from time-resolved diagnostic arrays at each sample point t. The diagnostic-confidence-corrected margin is:

$$m_{\mathrm{edge,conf}}(t) = f\left(m_{\mathrm{edge,raw}}(t),\, Q_{\mathrm{diag}}(t),\, P_{\mathrm{miss}}(t)\right), \tag{8}$$

where $Q_{\mathrm{diag}}(t) \in [0, 1]$ is the diagnostic quality score and $P_{\mathrm{miss}}(t)$ is the fraction of critical diagnostics missing at time t. The function f penalizes intervals with incomplete diagnostic support, preventing incomplete-coverage windows from generating inflated positive-margin readings.

3.6 Computational Research Corpus and Methodological Sequence

All derived numerical results reported in this manuscript are generated through the UNNS-H Mode Project computational archive [C1], using the external TCV and TokaMark/MAST data sources listed in the References. The archive provides a self-contained project structure containing adapters, chamber inputs, processed data products, analysis components, reports, dashboards, and manifests. The methodological sequence is:

1. TCV source ingestion through `tcv_zenodo_adapter.py`;
2. canonical event-table construction in `data/processed/`;
3. STRUC-I v1.0.4 admissibility preparation through chamber inputs;
4. STRUC-PERC-I v2.5.0 scalar-ladder and fragment-isolate preparation;
5. fragment-isolate mapping and suspect-shot review;
6. event-level edge-admissibility scoring (v0.1, nine reviewed shots);
7. full 92-event tag-free extension (v0.2);
8. TokaMark/MAST metadata scanning and $m_{\mathrm{edge}}(t)$ probing;
9. diagnostic-confidence correction ($m_{\mathrm{edge,conf}}(t)$);
10. physical-window labeling, hardening, and H-mode-stable recovery.

This corpus is the methodological basis for the validation tables, margin states, physical-window gate, and dashboard results reported in the manuscript.

4 TCV Event-Level Results: Nine-Shot Pilot

4.1 Data and Suspect-Shot Review

The TCV L-H threshold database (Zenodo record 14996664) contains discharge data for deuterium, hydrogen, helium, and mixed ion species from the TCV tokamak. A canonical event table of 92 rows was ingested via `tcv_zenodo_adapter.py`, yielding 66 unique shots with ILH labels (1 = H-mode obtained; 0 = not obtained).

A fragment-isolate mapping stage identified suspect-transition events through gap-structure analysis of the canonical table (569 KB fragment map). Nine events were then manually reviewed for physical consistency, producing a reviewed subset with branch-family tags: `power_balance`, `transport`, `timing`, and `edge_divertor_response`.

4.2 Strict Ordering Validation

The event-level margin $m_{\mathrm{edge,event}}$ was computed for all nine reviewed shots. The per-shot results are shown in Table 3.

Table 3: Per-shot event-level margin results for the nine reviewed TCV shots, ordered from most negative to most positive.

Shot	ILH	$m_{\mathrm{edge,event}}$	State	Branch family	Support
69807	0	−0.794	neg. leakage	power + transport + timing	strong neg.
69668	0	−0.552	neg. leakage	transport + timing	strong neg.
67992	1	−0.258	neg. leakage	power + transport	moderate neg.
68001	1;0	−0.227	neg. leakage	power + transport	moderate neg.
69913	1	−0.074	bdy. ambiguous	timing dominant	ambiguous
68206	1	+0.052	bdy. ambiguous	power balance	ambiguous
66445	1	+0.528	pos. boundary	edge divertor response	strong pos.
69892	1	+0.658	pos. boundary	edge divertor response	strong pos.
68719	1	+0.793	pos. boundary	edge divertor response	strong pos.

Finding 4.1 (Strict Ordering — TCV Nine-Shot Pilot). The three margin states are non-overlapping with a clear ordering gap:

$$\max(\text{negative leakage}) = -0.227 \;<\; \min(\text{boundary ambiguous}) = -0.074, \quad (9)$$

$$\max(\text{boundary ambiguous}) = +0.052 \;<\; \min(\text{positive boundary}) = +0.528. \quad (10)$$

The gap between the ambiguous maximum and the positive minimum is 0.476 margin units. The validation status is **PASS_STRICT_ORDERING**.

The state-level summary statistics are shown in Table 4.

Table 4: State-level margin statistics for the nine reviewed TCV shots.

State	n	**Mean**	**Min**	**Max**	**Std**
Negative leakage	4	−0.458	−0.794	−0.227	0.267
Boundary ambiguous	2	−0.011	−0.074	+0.052	0.089
Positive boundary	3	+0.660	+0.528	+0.793	0.133

4.3 Branch-Family Structure

Table 5 shows the mean margin by branch family. The decisive structural contrast is between the three leakage branches and the edge-divertor response branch.

Table 5: Mean event-level margin by branch family. Leakage branches occupy the negative side; edge-divertor response occupies the positive side.

Branch family	n	$\langle m_{\text{edge,event}} \rangle$	$\langle C_{\text{edge}} \rangle$	$\langle F_{\text{route}} \rangle$	$\langle S_{\text{er}} \rangle$	$\langle S_{\text{tr}} \rangle$
timing	3	−0.473	0.144	0.617	0.042	0.676
transport	4	−0.458	0.323	0.781	0.169	0.980
power_balance	4	−0.307	0.430	0.737	0.210	0.784
edge_divertor_resp.	3	+0.660	0.821	0.161	0.970	0.106

Finding 4.2 (Edge-Response Structural Distinctness). The edge-divertor response branch is structurally inverted relative to the leakage branches. Its mean $S_{\text{er}} = 0.970$ (versus ≤ 0.210 for all leakage branches) and mean $S_{\text{tr}} = 0.106$ (versus ≥ 0.676) demonstrate that it is not merely a lower-power leakage case: it occupies the opposite structural regime. The branch-mean gap between the weakest leakage branch and the edge-response branch is +0.967 margin units.

Figure 1 shows the nine shots on the $m_{\text{edge,event}}$ axis.

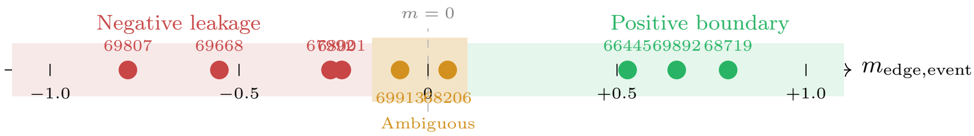

Figure 1: The nine reviewed TCV shots on the $m_{\text{edge,event}}$ axis (scale: 5 units = 1.0). Red dots: negative leakage margin. Amber dots: boundary ambiguous. Green dots: positive boundary margin. The three zones are non-overlapping with a gap of 0.476 units between the ambiguous maximum and the positive minimum.

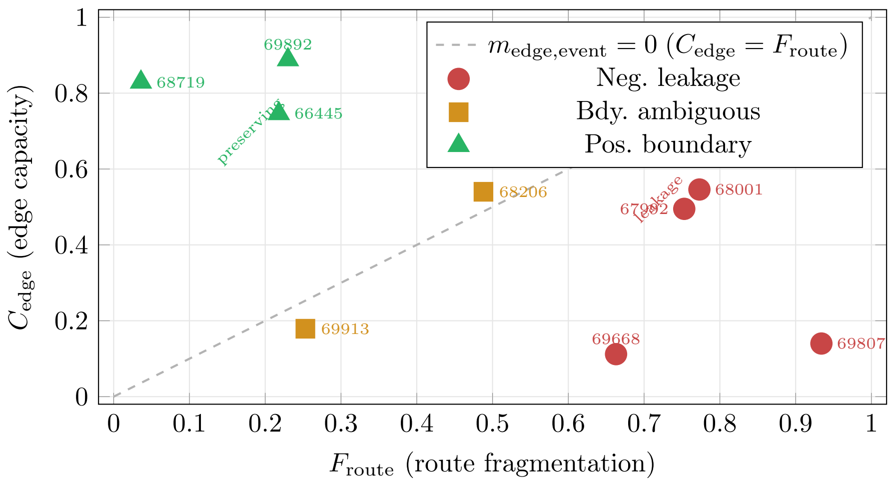

Figure 2: F_{route} versus C_{edge} for all nine reviewed TCV shots. Points above the dashed diagonal ($C_{\text{edge}} = F_{\text{route}}$) have positive margin; below have negative margin. The three positive-boundary shots (triangles) cluster in the high-C_{edge}, low-F_{route} quadrant; negative-leakage shots (circles) cluster in the high-F_{route}, low-C_{edge} quadrant; the two ambiguous shots (squares) sit near the diagonal. The structural inversion between the positive-boundary and negative-leakage clusters spans approximately 0.9 units in each axis.

5 TCV Full-Corpus Extension

5.1 Tag-Free Generalization

The nine-shot pilot relied on fragment-family tags from the manual review. The 92-event full corpus does not have such tags for every event. A tag-free numerical generalization of the model (v0.2) uses the same formula (1)–(3) without branch-family tag assistance.

The full corpus contains 92 event rows from 66 unique shots (ILH=1: 84; ILH=0: 8).

5.2 State Distribution

The full corpus distributes across states as shown in Table 6.

Table 6: State-level distribution in the 92-event TCV full corpus (v0.2 tag-free generalization).

State	n	Mean	Median	Min	Max	95% CI	ILH= 1 rate
Boundary ambiguous	68	−0.038	−0.055	−0.199	+0.182	[−0.061, −0.015]	0.956
Negative leakage	11	−0.356	−0.285	−0.664	−0.207	[−0.450, −0.270]	0.636
Positive boundary	13	+0.341	+0.312	+0.223	+0.585	[+0.297, +0.395]	0.923

The dominant state is boundary ambiguous (74%), which is physically expected for a transition event table: most events sit near the admissibility threshold rather than deeply within a leakage or confinement regime.

Finding 5.1 (Full-Corpus Three-Corridor Persistence). The three-corridor structure persists in the 92-event tag-free generalization. The margin shows real ILH association: AUC = 0.690, mean ILH= 1 minus ILH= 0 difference = +0.242, permutation p = 0.0022. The confidence intervals of the three states do not overlap.

5.3 Comparison with Standard Plasma Variables

Table 7 compares the leave-one-out (LOO) AUC for ILH= 1 of standard plasma variable classifiers and the UNNS margin.

Table 7: Leave-one-out AUC for ILH= 1 for logistic regression classifiers using standard plasma variables and the UNNS margin.

Model	Features	LOO AUC
Standard core	P_{LH}, P_{tot}, P_{loss}, n_e, I_p, B_t, q_{95}, κ, δ, n_{Ryter}, ...	1.000
Standard core + $m_{\text{edge,event}}$	Above + $m_{\text{edge,event}}$	1.000
Standard edge inclusive	Above + χ_{eff}, divertor signals	1.000
UNNS components	S_{pb}, S_{tr}, S_{er}, S_{ti}, F_{route}, C_{edge}	0.696
UNNS margin only	$m_{\text{edge,event}}$	0.655

Remark 5.2 (UNNS Contribution is Structural, not Predictive). Standard plasma variables classify ILH at LOO AUC = 1.000; adding $m_{\text{edge,event}}$ does not improve binary ILH prediction. Because the ILH= 0 class contains only 8 of 92 events, the perfect standard-variable AUC should be interpreted as dataset-specific separability rather than a general prediction claim. This does not invalidate the UNNS result. The UNNS contribution at this stage is *structural organization*: $m_{\text{edge,event}}$ reorganizes the event table into leakage-like, boundary-ambiguous, and edge-response corridors, revealing how power-balance, transport, timing, and edge-response terms oppose each other in an event-level boundary-admissibility model. It is not a replacement for standard variables.

5.4 Statistical Separation and Effect Size

The three-state separation in the 92-event corpus is numerically large and descriptively stable. A Kruskal–Wallis test across the three margin-state groups yields $H = 53.85$ (df = 2, $p \ll 0.001$), confirming that the between-group differences in $m_{\text{edge,event}}$ are not attributable to sampling noise.

Effect sizes (Cohen's d) for pairwise contrasts are large in all cases:

Contrast	Cohen's d	Interpretation
Positive vs. negative leakage	5.33	very large
Positive vs. boundary ambiguous	3.90	very large
Ambiguous vs. negative leakage	2.93	very large

In the nine-shot pilot, the edge-response branch (mean +0.660, $n = 3$) versus the pooled leakage branches (mean −0.309, $n = 6$) gives Cohen's $d = 3.54$.

Remark 5.3. With $n = 9$ reviewed shots and $n = 92$ full-corpus events (84 ILH= 1, 8 ILH= 0), these statistics should be read as supportive diagnostics rather than definitive proof of general separation. The large effect sizes reflect the structural contrast already visible in the raw margin values; they do not establish that the same separation will persist in a balanced or externally validated corpus.

6 TokaMark Time-Resolved Extension

6.1 Data Access and Candidate Selection

TokaMark/MAST data is accessible through public HTTP metadata and chunk-level diagnostic array endpoints. A metadata candidate scan identified shots with complete coverage of profile, edge, power, density, and geometry diagnostics. Shot 12063 was identified as the highest-ranked candidate from this scan and from a subsequent five-shot moderated-confidence panel comparison.

The five-shot panel ranking was: 12063 (rank 1, structurally strongest), 11876 (rank 2), 11776 (rank 3, confidence-limited), 11768 (rank 4, confidence-limited), 11830 (rank 5, weakest).

6.2 First m_edge(t) Trace

Shot 12063 yielded the first time-resolved UNNS-H Mode margin trace from public TokaMark/MAST data. The v0.1 trace was predominantly boundary-ambiguous with positive-boundary excursions and negative-leakage intervals, demonstrating that the margin is not trivially positive-labeling across the full discharge. Positive windows showed $C_{\text{edge}} > F_{\text{route}}$ with edge-response contribution and reduced power-balance pressure. Negative windows showed elevated transport and power-balance fragmentation.

6.3 Diagnostic-Confidence Correction

Shots 11776 and 11768 showed inflated positive-boundary fractions in the v0.1 margin despite missing critical diagnostics. The v0.1 margin conflates structural edge-capacity signal with diagnostic absence (reduced fragmentation evidence in incomplete shots).

To address this, a diagnostic-confidence correction was introduced [U4, U15]:

$$m_{\text{edge,conf}}(t) \;=\; f(m_{\text{edge,raw}}(t),\, Q_{\text{diag}}(t),\, P_{\text{miss}}(t))\,, \tag{11}$$

where $Q_{\text{diag}}(t)$ is the diagnostic quality score based on coverage of NBI power, D-alpha, Thomson scattering T_e/n_e, soft-X emission, transport term, and geometry support; and $P_{\text{miss}}(t)$ penalizes windows with missing critical diagnostic fields. The $m_{\text{edge,conf}}$ correction preserves shot 12063's structural signal while suppressing the inflated positives in 11776 and 11768.

7 Physical-Window Labeling and Hardening

7.1 Window Construction

Time-resolved traces from TokaMark/MAST were segmented into analysis windows [U13, U14]. Each window was assigned one of four labels based on physical diagnostic evidence:

- L_MODE: pre-transition baseline window; D-alpha and edge-emission remain at their pre-event level, before the suppression or change associated with transition; profile sharpening absent; high route-fragmentation indicators;
- LH_TRANSITION: L-H transition window, spanning the event time; localized change or onset of D-alpha or edge-emission suppression near the transition time; intermediate indicators;
- H_MODE_STABLE: post-transition interval with sustained altered or suppressed D-alpha behavior consistent with reduced edge recycling, together with edge-profile-gradient support and soft-X consistency;
- UNLABELABLE: insufficient diagnostic coverage; excluded from analysis.

7.2 Conservative Hardening (v0.1) and Recovery (v0.2)

An initial conservative pass (HARDENED_v0.1) suppressed all H_MODE_STABLE windows that lacked external anchoring to shot-log or publication L-H timing records. This produced a valid but overly conservative label set.

The v0.2 recovery gate restored H_MODE_STABLE windows that had sufficient *independent* *internal* physical evidence from D-alpha, profile-gradient, soft-X, and power-density context fields. The non-circularity rule was strictly enforced: labels were assigned from physical evidence fields only; UNNS margin columns were examined only after labeling to test alignment.

Principle 7.1 (Non-Circularity)**.** Physical window labels must be assigned from physical diagnostic evidence before comparison to the UNNS margin. The margin is not used as evidence for labeling. The comparison is a test, not a construction.

The v0.2 recovery gate produced 17 eligible windows from 89 total (72 excluded as UNLABELABLE or uncovered):

- 6 L_MODE windows from 6 shots;
- 6 LH_TRANSITION windows from 6 shots;
- 5 H_MODE_STABLE windows from 5 shots.

Hardening level: **2_SUPPORTED** — internally consistent, not yet externally anchored to expert-reviewed L-H transition timing.

8 Main Physical-Window Result

8.1 By-Label Result

Table 8 reports the median $m_{\text{edge,conf}}$ and key diagnostic quality indicators for each label type across the recovered window set.

Table 8: By-label summary of $m_{\text{edge,conf}}$ medians and diagnostic quality indicators (HARDENED_v0.2, 17 eligible windows). Medians are taken over the per-shot window medians.

Label	Win.	Shots	Dur. (s)	Median $m_{\text{edge,conf}}$	conf+ frac.	Median Q_{diag}
L_MODE	6	6	0.390	−1.120	0	0.06
LH_TRANSITION	6	6	0.115	−0.289	0	0.889
H_MODE_STABLE	5	5	0.336	+0.053	0.261	1.000

The ordering

$$\text{L\_MODE} < \text{LH\_TRANSITION} < \text{H\_MODE\_STABLE} \tag{12}$$

is confirmed in the median $m_{\text{edge,conf}}$: $-1.120 < -0.289 < +0.053$.

Remark 8.1 (Diagnostic Floor). The L_MODE median $m_{\text{edge,conf}} = -1.120$ reflects the diagnostic-confidence floor for this first recovered window set. All six L_MODE windows have poor diagnostic quality ($Q_{\text{diag}} = 0.06$) and maximum missing-critical-field scores ($P_{\text{miss}} = 1.0$). The separation between L_MODE and H_MODE_STABLE should therefore be read as a confidence-corrected structural separation, not a raw-margin separation. The within-shot comparison in Section 8.2 controls for this confound.

8.2 Within-Shot L-to-H Recovery

Table 9 reports the within-shot comparison: for each of the five shots with both L_MODE and H_MODE_STABLE windows, the per-shot medians and their difference Δ = H_STABLE − L_MODE.

Finding 8.2 (Within-Shot L-to-H Ordering). In every shot where both L_MODE and H_MODE_STABLE windows are recovered, the H_MODE_STABLE window has a strictly higher $m_{\text{edge,conf}}$ median than the L_MODE window from the same shot. The within-shot

Table 9: Within-shot $m_{\text{edge,conf}}$ medians for L-mode and H-mode-stable windows, and the H-minus-L delta. All five within-shot deltas are positive.

Shot	L-mode	LH-trans.	H-stable	Δ (H−L)	conf+
12007	−1.120	−0.174	−0.038	+1.082	0
12017	−1.120	−0.030	−0.058	+1.062	0
12046	−1.120	−0.498	+0.206	+1.326	0.514
12055	−1.120	−0.265	+0.196	+1.316	0.481
12063	−1.120	−0.313	+0.053	+1.173	0.261

H-minus-L deltas are positive in all five cases, with values +1.082, +1.062, +1.326, +1.316, and +1.173. The minimum delta is +1.062.

Figure 3 illustrates the label ordering.

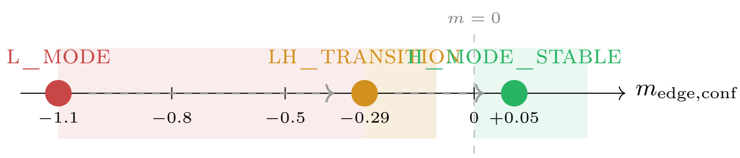

Figure 3: Median $m_{\text{edge,conf}}$ for the three label types in the HARDENED_v0.2 window set. The ordering L_MODE < LH_TRANSITION < H_MODE_STABLE is confirmed. The L_MODE median (−1.120) is at the diagnostic-confidence floor; see Remark 8.1 and Section 8.2 for the within-shot comparison that controls for this.

8.3 Gate Decision

The v0.2 physical-window analysis passes the first gate:

decision: physical_window_analysis_passes_first_gate

with the following criteria met:

- Both L_MODE and H_MODE_STABLE labels are present.
- LH_TRANSITION labels are present for transition-local comparison.
- H_MODE_STABLE windows have higher median $m_{\text{edge,conf}}$ than L_MODE windows.
- H_MODE_STABLE windows have higher or equal confidence-positive fraction.
- Most within-shot H_MODE_STABLE windows have higher $m_{\text{edge,conf}}$ than L_MODE windows.
- UNLABELABLE windows are excluded.

The result does not yet constitute full physical validation. The label hardening level is **2_SUPPORTED**: internally consistent physical evidence but not externally anchored to expert-reviewed or publication-verified L-H transition timing.

9 Discussion

9.1 H-Mode as Boundary-Route Preservation

The empirical results across three layers support a coherent structural interpretation of H-mode.

In the TCV event-level analysis, the positive-boundary corridor is defined not by high total heating power but by edge-response dominance. The three positive-boundary shots (66445, 69892, 68719) share $S_{\text{er}} \geq 0.945$ and $S_{\text{tr}} \leq 0.182$ — the opposite signature of the negative-leakage shots, which have $S_{\text{tr}} \geq 0.960$ and $S_{\text{er}} \leq 0.287$. This structural inversion suggests that the transition to H-mode involves a change in the *type* of edge activity, not only in its magnitude.

In the TCV full-corpus extension, the margin has real ILH association (AUC = 0.690, permutation $p = 0.0022$) but standard variables remain superior for binary prediction. This is not a failure of the structural account; it reflects that binary ILH prediction in this event table is already saturated by standard variables. The structural contribution is different: it provides a decomposition of the L-H event into fragmentation and capacity channels that carries physical interpretive content [U9, U10, U11, U12].

In the TokaMark/MAST physical-window analysis, within-shot L-to-H deltas are positive in all five recovered cases. This within-shot comparison is more informative than the across-shot comparison because it controls for shot-specific structural baselines. The consistency of the positive within-shot deltas (+1.062 to +1.326) across five independent discharges is the strongest result in this paper.

This is the plasma-domain version of the charge-domain pattern described in Section 2.3: visible balance or access is not sufficient; admissibility depends on route preservation.

This constitutes a theoretical gain for the UNNS Substrate program. The result does not claim universal validation in the absolute sense. Rather, it demonstrates a cross-domain recurrence of the same structural law-form: a visible scalar, label, or balance condition is necessary but not sufficient, while boundary-route preservation supplies the admissibility condition. In the charge domain, the visible projection is scalar charge balance and the structural invariant is route/closure preservation. In the plasma domain, the visible projection is threshold access or binary H-mode classification, while the structural invariant is edge-route preservation. The same law-form therefore appears in two physically distinct settings: charge-bearing particle transitions and macroscopic plasma-boundary confinement. This supports the interpretation of UNNS universality as law-form recurrence across domains, backed by domain-specific empirical constructions.

9.2 Interpretive Case Studies

The three case studies below use component values drawn directly from `tcv_edge_event_model_scores.csv` in the research corpus [C1]. They illustrate what the structural coordinate reveals beyond binary ILH prediction.

Shot 68001 — ILH= 1;0, negative leakage, $m_{\text{edge,event}} = -0.227$. This shot has two canonical event rows with conflicting ILH labels (H-mode obtained in one time window, not in another). The margin assigns it to the negative leakage corridor: $S_{\text{pb}} = 0.989$, $S_{\text{tr}} = 0.973$, $S_{\text{er}} = 0.287$, $F_{\text{route}} = 0.773$, $C_{\text{edge}} = 0.546$. High power-balance and transport pressure dominate the event despite a moderate edge response and a density-supportive setting. The structural reading is that this shot reaches or briefly crosses the H-mode threshold but does so in a structurally fragmentation-loaded configuration — consistent with the mixed ILH outcome.

Shot 67992 — ILH= 1, negative leakage, $m_{\text{edge,event}} = -0.258$. This shot is scored ILH= 1 (H-mode obtained) but sits in the negative leakage corridor. Its component values are: $S_{\text{pb}} = 0.961$, $S_{\text{tr}} = 0.960$, $S_{\text{er}} = 0.282$, $F_{\text{route}} = 0.753$, $C_{\text{edge}} = 0.495$. Power-balance and transport pressure are near-maximal; edge response is low. The structural interpretation is that H-mode was obtained under high fragmentation load — the boundary was crossed by brute heating rather than edge reorganization. This is the clearest case where the structural and binary-ILH classifications diverge: the predictive outcome is positive, but the structural coordinate places the event at the fragmentation-dominated end of the ILH= 1 set.

Shot 66445 — ILH= 1, positive boundary, $m_{\text{edge,event}} = +0.528$. This shot is the cleanest of the three positive-boundary cases: all diagnostic fields are present with no missing χ_{eff} or P_{loss}. Its component values are: $S_{\text{pb}} = 0.240$, $S_{\text{tr}} = 0.135$, $S_{\text{er}} = 0.970$, $S_{\text{ti}} = 0.290$, $F_{\text{route}} = 0.218$, $C_{\text{edge}} = 0.746$. Power-balance and transport scores are moderate rather than suppressed, but edge-response dominance ($S_{\text{er}} = 0.970$) is sufficient to produce a strongly positive margin. The structural reading is that this shot approaches H-mode through a configuration where edge capacity definitively exceeds fragmentation pressure across all fully diagnosed channels. The contrast with shots 67992 and 68001 — where $F_{\text{route}} > 0.75$ despite ILH= 1 — illustrates that the UNNS corridor assignment captures a genuine structural distinction within the ILH= 1 population.

9.3 Relation to Standard Plasma Physics

The UNNS edge-admissibility margin is not in conflict with standard plasma physics. Power, density, effective transport, and geometry all appear as components of F_{route} and C_{edge}. The structural account proposes that these quantities are better understood as a balance between fragmentation pressure and edge capacity than as a single threshold.

The candidate edge-response signal S_{er} used in this analysis is a proxy for the combined effect of D-alpha suppression, profile sharpening, and divertor-state changes. It is not independently identified as radial electric field formation or $E \times B$ shear. A rigorous identification would require direct measurement of E_r or the $E \times B$ rotation profile, which is beyond the scope of the present analysis.

9.4 Diagnostic Confidence and its Role

The diagnostic-confidence correction $m_{\text{edge,conf}}(t)$ was essential for obtaining interpretable TokaMark results. Without confidence weighting, shots 11776 and 11768 produced inflated positive-margin readings driven by diagnostic absence rather than genuine edge-response structure. The correction demonstrates that the v0.1 margin must be treated with caution in incomplete-diagnostic settings until confidence weighting is fully validated.

10 Limitations and Next Work

The present work establishes an empirical UNNS formulation of H-mode as boundary-route preservation, with internally supported results across three data layers. Four limitations define the boundary of the current claim.

External anchoring. The five recovered H_MODE_STABLE windows are 2_SUPPORTED (internally consistent) but not 3_EXTERNALLY_ANCHORED. The next required step is to compare the recovered H_MODE_STABLE window intervals for shots 12007, 12017, 12046, 12055, and 12063 against expert-reviewed shot-log or publication L-H transition timing. If external timing is unavailable, a falsification panel of diagnostic-complete shots where no H-mode is expected provides an alternative test.

TCV positive-boundary corridor time traces. Full corridor-resolved time validation requires a time-resolved positive-boundary TCV trace for at least one of shots 66445, 69892, or 68719. These shots lie in the positive boundary corridor but are not yet covered by the available `LH_DATA.h5` inventory.

Time-series edge diagnostics. The full time-dependent edge margin $m_{\text{edge}}(t)$ has not been validated against direct edge turbulence, radial electric field, $E \times B$ shear, pedestal gradient evolution, confinement time response, or ELM timing data. This is required before the time-resolved margin can be claimed as a physical proxy for the edge transport barrier.

Cross-machine replication. All results are from TCV and one MAST dataset. Cross-machine replication on a second machine (FAIR MAST, AUG, DIII-D, or JET) is required before any claim of structural universality.

11 Conclusion

We have presented a UNNS edge-admissibility analysis of plasma H-mode as a boundary-route preservation transition. The central result is that a confidence-corrected edge-admissibility margin $m_{\text{edge,conf}}$ orders plasma transition data consistently across three empirical layers:

1. **TCV event-level corridors**: nine reviewed TCV shots separate into strictly non-overlapping negative leakage, boundary ambiguous, and positive boundary corridors; the positive corridor is defined by edge-response dominance, not heating power alone.
2. **TCV full-corpus extension**: the three-corridor structure persists in the 92-event tag-free generalization, with real ILH association (AUC = 0.690, permutation $p = 0.0022$).
3. **TokaMark physical-window recovery**: HARDENED_v0.2 physical windows recover the ordering L_MODE < LH_TRANSITION < H_MODE_STABLE under $m_{\text{edge,conf}}$, with positive within-shot H-minus-L deltas in all five recovered H-mode-stable cases (minimum +1.062).

A further gain is cross-domain structural alignment. The plasma result recovers the same UNNS law-form previously extracted in charge-boundary routing: value or access is a visible projection, while admissibility depends on preservation of the underlying route. The H-mode analysis therefore extends boundary-route preservation from charge-bearing transitions to time-dependent plasma confinement.

The manuscript's central claim, in its one-sentence form, is:

Central Thesis. *H-mode plasma confinement can be represented as a boundary-route preservation transition in which the plasma edge moves from fragmentation-dominated leakage toward an admissible route-preserving state, and this transition is empirically reflected in UNNS edge-admissibility margins across TCV event corridors and TokaMark physical windows.*

This work establishes a first empirical UNNS formulation of H-mode as boundary-route preservation. External anchoring of the physical windows, TCV positive-boundary time traces, time-series edge diagnostic validation, and cross-machine replication are the required next steps before this formulation can be promoted to a validated physical claim.

A Symbol Glossary

Symbol	**Meaning**
$m_{\text{edge,event}}$	Event-level edge-admissibility margin
$m_{\text{edge}}(t)$	Time-resolved edge-admissibility margin
$m_{\text{edge,conf}}(t)$	Diagnostic-confidence-corrected margin
$m_{\text{edge,raw}}(t)$	Raw (uncorrected) time-resolved margin
F_{route}	Route-fragmentation pressure
C_{edge}	Edge-preserving capacity
S_{pb}	Power-balance score
S_{tr}	Transport score
S_{er}	Edge-response score
S_{ti}	Timing score
ρ_{dens}	Density support percentile
γ_{geom}	Geometry stability term
σ_{sp}	Species position term
$Q_{\text{diag}}(t)$	Diagnostic quality score
$P_{\text{miss}}(t)$	Missing-critical-field fraction
ILH	L-H indicator (1 = H-mode obtained; 0 = not)
AUC	Area under the ROC curve (vs. ILH= 1)
L_MODE	L-mode physical window label
LH_TRANSITION	L-H transition physical window label
H_MODE_STABLE	H-mode-stable physical window label

B Score Construction and Normalization

Each score component is normalized to $[0, 1]$ before use in equations (2) and (3). The normalization is corpus-relative: percentiles and robust scaling are computed over the full 92-event TCV canonical table (`tcv_lh_events_canonical.csv`).

S_{pb} **(power-balance score).** Derived from the ratio of total heating power to the Ryter threshold ($P_{\text{total}}/P_{\text{Ryter}}$) and the power-loss pressure ($P_{\text{loss}}/P_{\text{LH}}$). High values indicate that heating and loss power are both elevated relative to threshold, corresponding to high fragmentation pressure. Mapped to $[0, 1]$ by min-max scaling over the full corpus.

S_{tr} **(transport score).** Derived from effective transport elevation (χ_{eff} candidate) and power-loss pressure. High values correspond to elevated transport coefficients consistent with a leakage-dominated edge. Mapped to $[0, 1]$ by robust scaling (5th–95th percentile clip) over the full corpus.

S_{er} **(edge-response score).** Derived from the candidate divertor/edge response signal (`divertor_signal_candidate` and `divertor_signal_150_candidate`). High values indicate a strong edge/divertor response consistent with transition-associated boundary reorganization. Mapped to $[0, 1]$ by min-max scaling; the signal is confirmed as a candidate proxy only (D-alpha source-field identification requires source notebook verification).

S_{ti} **(timing score).** Derived from the spread and consistency of transition-event timing indicators (`event_time` spread, multi-indicator consistency). High values correspond to fragmented or inconsistent transition timing. Mapped to $[0, 1]$ via percentile position in the full corpus.

ρ_{dens} **(density support).** Percentile position of line-averaged electron density n_e relative to the Ryter density threshold n_{Ryter} in the full corpus. High values correspond to favorable density positioning.

γ_{geom} **(geometry stability).** Composite of q_{95}, κ (elongation), and δ (triangularity) percentile positions relative to the full corpus. Weighted average scaled to $[0, 1]$.

σ_{sp} **(species position).** Derived from hydrogen and helium fraction candidates. Positioned relative to deuterium-equivalent baseline. Mapped to $[0, 1]$ by min-max scaling.

The v0.1 (nine-shot) model used tag-assisted branch-family weights. The v0.2 (92-event) generalization used the fixed weights $F = 0.35\,S_{\text{pb}} + 0.35\,S_{\text{tr}} + 0.30\,S_{\text{ti}}$ and $C = 0.45\,S_{\text{er}} + 0.25\,\rho_{\text{dens}} + 0.15\,\gamma_{\text{geom}} + 0.15\,\sigma_{\text{sp}}$ without per-event branch tags. These weights are fixed as of v0.2 and are not tuned after seeing validation results; see the reproducibility bundle (Appendix C) for the implementing script.

C Reproducibility Bundle

The reproducibility bundle is contained in the public research corpus [C1]. The archive contains the project manifest, README files, adapters, processed data products, STRUC-I and STRUC-PERC-I chamber inputs, analysis components, reports, dashboards, and validation outputs required to reproduce the manuscript's computational pathway.

The following scripts implement the analysis pipeline. All scripts are in `unns_hmode_project/components/` and operate on data in `unns_hmode_project/data/` and outputs in `unns_hmode_project/outputs/`, as distributed in [C1].

Script	**Function**
`tcv_zenodo_adapter.py`	Ingest TCV Zenodo 14996664
`tcv_fragment_isolate_mapper.py`	Fragment-isolate mapping
`tcv_suspect_shot_reviewer.py`	Suspect-shot selection
`edge_admissibility_event_model.py`	v0.1 event-level margin
`edge_event_model_validator.py`	Strict-ordering validation
`full_corpus_edge_event_extension.py`	v0.2 tag-free generalization
`tokamark_metadata_candidate_scanner.py`	TokaMark candidate scan
`tokamark_m_edge_t_probe.py`	$m_{\text{edge}}(t)$ first trace
`tokamark_m_edge_confidence_revision.py`	$m_{\text{edge,conf}}(t)$ correction
`tokamark_physical_window_label_analyzer.py`	Window labeling
`tokamark_physical_label_hardening_template.py`	v0.1→v0.2 hardening
`tokamark_hmode_stable_evidence_reviewer.py`	H-mode-stable recovery

Key output files required to reproduce the main results:

- `tcv_edge_event_model_validation_summary.json` (nine-shot strict-ordering result);
- `tcv_full_corpus_edge_event_summary.json` (92-event state distribution and AUC);
- `tokamark_physical_window_label_analysis_HARDENED_v0_2.json` (by-label and within-shot window results).

D Weight Sensitivity and Robustness

The nominal weights in equations (2) and (3) are $\mathbf{w}_F = (0.35, 0.35, 0.30)$ and $\mathbf{w}_C = (0.45, 0.25, 0.15, 0.15)$. This appendix reports the result of perturbing each weight individually by ±10%, ±20%, and ±30% (normalized to sum to unity after perturbation) and testing whether strict ordering of the three corridors is preserved.

Test set: all nine reviewed TCV shots with exact component values from `tcv_edge_event_model_scores.csv` [C1]. The strict-ordering criterion requires $\max(\text{neg}) < \min(\text{amb})$ and $\max(\text{amb}) < \min(\text{pos})$.

Perturbation level	Trials	Strict ordering preserved
±10% (all single-weight)	14	14 / 14
±20% (all single-weight)	14	14 / 14
±30% (all single-weight)	14	14 / 14

Under all 14 tested single-weight perturbations at ±30%, the original pilot groups remain strictly ordered: the negative-leakage group remains below the ambiguous group, and the ambiguous group remains below the positive-boundary group.

- The edge-response branch separation: $S_{\text{er}} \pm 30\%$ gives $\max(\text{neg}) \in [-0.258, -0.187]$, $\max(\text{amb}) \in [0.013, 0.104]$, $\min(\text{pos}) \in [0.493, 0.554]$ — ordered in all cases. One boundary-ambiguous case approaches or slightly exceeds the nominal +0.10 threshold under the S_{er} +30% perturbation, but remains far below the positive-boundary cluster (minimum gap $0.493 - 0.104 = 0.389$).
- Shots 66445, 69892, and 68719 remain well within the positive-boundary corridor ($m_{\text{edge,event}} > 0.49$) under every tested perturbation; none approaches the ambiguous zone.

The robust result is therefore ordered group separation, not absolute invariance of every threshold label.

Remark D.1. This analysis tests single-weight perturbations only. Combined or adversarial multi-weight perturbations, or perturbations exceeding ±30%, are not tested here. The results establish that the nine-shot strict ordering is not a thin-margin artifact of the nominal weight choice, but they do not establish robustness to arbitrary weight changes. External anchoring of the corridor assignment to physical diagnostics remains the appropriate validation pathway.

E Data Provenance

All provenance entries below refer to files contained in the UNNS-H Mode Project Research Corpus [C1], unless otherwise noted.

Stage	**Output**	**Status**
TCV ingestion	`tcv_lh_events_canonical.csv`	Complete
STRUC-I v1.0.4 baseline	`struc_i_results.json`	Complete
STRUC-PERC-I v2.5.0 batch	`struc_perc_batch_results.*`	Complete
Fragment-isolate mapping	`tcv_fragment_gap_map.csv`	Complete
Suspect-shot review	`tcv_suspect_shot_review.csv`	Complete
Manual physical review	`TCV_Manual_Review.csv`	Complete
Event-level model (v0.1)	`edge_event_model_scores.csv`	Complete
9-shot validation	PASS_STRICT_ORDERING	Complete
Full corpus extension (v0.2)	`tcv_full_corpus_scores.csv`	Complete
Standard-variable comparison	`full_corpus_std_vs_unns.csv`	Complete
TokaMark metadata scan	Doc 17: candidate shot inventory	Complete
TokaMark $m_{\text{edge}}(t)$ probe	Doc 19: shot 12063 first trace	Complete
5-shot panel	Doc 27: 12063 ranked #1	Complete
Physical window labeling	L_MODE / LH_TRANSITION / H_MODE_STABLE	Complete
Label hardening v0.1→v0.2	HARDENED_v0.2 labels	Complete
H-mode-stable recovery	Doc 33: 5 shots, Gate 1 PASS	Complete
External anchoring	Doc 34 (planned)	Next
TCV pos.-boundary trace	Shots 66445, 69892, 68719	Blocked
Cross-machine replication	FAIR MAST / AUG	Not yet

References

[1] F. Wagner, G. Becker, K. Behringer, D. Campbell, A. Eberhagen, W. Engelhardt, G. Fussmann, O. Gehre, J. Gernhardt, G. v. Gierke, G. Haas, M. Huang, F. Karger, M. Keilhacker, O. Klüber, M. Kornherr, K. Lackner, G. Lisitano, G. G. Lister, H. M. Mayer, D. Meisel, E. R. Müller, H. Murmann, H. Niedermeyer, W. Poschenrieder, H. Rapp, H. Röhr, F. Schneider, G. Siller, E. Speth, A. Stäbler, K. H. Steuer, G. Venus, O. Vollmer, and Z. Yü. Regime of improved confinement and high beta in neutral-beam-heated divertor discharges of the ASDEX tokamak. *Physical Review Letters*, 49(19):1408–1412, 1982.

[2] F. Ryter, F. Bareyt, G. Tardini, H. Salzmann, R. Sartori, A. C. C. Sips, M. Sokoll, C. D. Thomas, K. Thomsen, and the ITER Power Threshold Database Working Group. H-mode power threshold and transition in ASDEX upgrade. *Nuclear Fusion*, 36(11):1217–1232, 1996.

[3] Y. R. Martin, T. Takizuka, and the ITPA CDBM H-mode Threshold Database Working Group. Power requirement for accessing the H-mode in ITER. *Journal of Physics: Conference Series*, 123:012033, 2008.

[4] K. H. Burrell. Effects of E×B velocity shear and magnetic shear on turbulence and transport in magnetic confinement devices. *Physics of Plasmas*, 4(5):1499–1518, 1997.

[5] P. W. Terry. Suppression of turbulence and transport by sheared flow. *Reviews of Modern Physics*, 72(1):109–165, 2000.

[6] S. Coda, M. Agostini, R. Albanese, S. Alberti, E. Alessi, S. Allan, J. Allcock, R. Ambrosino, H. Anand, V. Anastassiou, Y. Andrew, and the TCV Team. Physics research on the TCV tokamak facility: from conventional to alternative scenarios and beyond. *Nuclear Fusion*, 59(11):112023, 2019.

[7] TCV L-H Threshold Transition Database. *Zenodo*, record 14996664, 2024. `https://doi.org/10.5281/zenodo.14996664`.

[8] J. W. Connor and H. R. Wilson. A review of theories of the L-H transition. *Plasma Physics and Controlled Fusion*, 42(1):R1–R74, 2000.

[9] M. Schmidtmayr, J. W. Hughes, F. Ryter, S. Saarelma, N. Cao, A. E. Hubbard, J. H. Irby, E. Marmar, M. L. Reinke, J. E. Rice, and S. G. Wolfe. Investigation of the critical edge ion heat flux for L-H transitions in Alcator C-Mod. *Nuclear Fusion*, 57(5):056002, 2017.

[10] C. F. Maggi, H. Weisen, J. C. Hillesheim, A. Chankin, E. Delabie, L. Frassinetti, F. Auriemma, I. S. Carvalho, G. Corrigan, J. Flanagan, and the JET Contributors. Isotope effects on L-H threshold and confinement in tokamak plasmas. *Nuclear Fusion*, 58(9):096029, 2018.

[11] I. T. Chapman, M. F. de Bock, J. R. Harrison, A. Kirk, M. Koscǎl, P. Naylor, S. D. Pinches, M. Turnyanskiy, S. Zoletnik, and the MAST Team. Overview of MAST results. *Nuclear Fusion*, 51(7):073040, 2011.

[12] TokaMark/TokaMind public data access. *TokaMark Online Repository*, 2024. `https://tokamark.tech`.

Research Corpus

[C1] UNNS Substrate Research Program. UNNS-H Mode Project Research Corpus: Boundary-Route Preservation in H-Mode Plasma. Computational archive, 2026. Available at: `https://unns.tech/media/unns/UNNS_plasma_H_Mode/unns_hmode_project.zip`.

UNNS Program Bibliography

The following UNNS Substrate manuscripts form the internal theoretical and methodological foundation for the present work. They are cited as program-corpus references rather than external plasma-physics references.

Instrumentation note. STRUC-I v1.0.4 and STRUC-PERC-I v2.5.0 are analysis instruments used in this project. They are documented in the reproducibility bundle and data provenance appendices (Appendices C and D) rather than cited as standalone theory manuscripts.

UNNS Corpus References

[U1] UNNS Substrate Research Program. Foundations of the UNNS Substrate: From Universal Admissibility to Structural Regime Theory. Foundation document, 2026.

[U2] UNNS Substrate Research Program. The Universal Structural Law v6. Working manuscript, 2026.

[U3] UNNS Substrate Research Program. The Percolative Realizability Principle: Realizability Structure of Admissible Configurations and the Revised Necessary Direction. Working manuscript, 2026.

[U4] UNNS Substrate Research Program. Structural Realizability and Dual Observability in the Admissibility Manifold: A Second Structural Layer Between Admissibility and

Dynamics. Working manuscript, 2026.

[U5] UNNS Substrate Research Program. Connectivity Margin as a Coordinate of Realizability Space: Monotonicity, Boundary Geometry, and Canonical Structure in the UNNS Substrate. Working manuscript, 2026.

[U6] UNNS Substrate Research Program. Local Geometry of Realizability Boundaries in the UNNS Substrate: From Connectivity Margin to Boundary Distance. Working manuscript, 2026.

[U7] UNNS Substrate Research Program. The Margin-Confinement Law: Structural Non-Crossability in Admissibility Space Derived from the Universal Structural Law and the Percolative Realizability Principle. Foundational theory manuscript, 2026.

[U8] UNNS Substrate Research Program. Admissible Boundary Routing: Structural Classification of Terminal Approach, Finite Bounce, and Cosmological Recession. Working manuscript, 2026.

[U9] UNNS Substrate Research Program. The Charge Boundary-Route Preservation Law: Value Conservation, Route Admissibility, and Structural Selection in Charge-Bearing Transitions. Completed manuscript, 2026.

[U10] UNNS Substrate Research Program. Admissible Cluster Geometry. Working manuscript, 2026.

[U11] UNNS Substrate Research Program. Canonical Structures in Admissibility Space. Working manuscript, 2026.

[U12] UNNS Substrate Research Program. Bounded Structural Rigidity and Representation-Driven Structure. Working manuscript, 2026.

[U13] UNNS Substrate Research Program. Structural Trajectories in Realizability Space: Voyager 2 Plasma as a Time-Resolved Test of the UNNS Substrate. Working manuscript, 2026.

[U14] UNNS Substrate Research Program. Structural Phase Transitions Along Physical Trajectories: Voyager Data as a Dynamic Realization of Realizability Geometry. Working manuscript, 2026.

[U15] UNNS Substrate Research Program. The UNNS Observability–Admissibility Duality Theorem. Working manuscript, 2026.

[U16] UNNS Substrate Research Program. Charge Boundary Routing: Fractional Coordinates, Composite Closure, and Route-Preserving Transitions. Working manuscript, 2026.